ADVANCED SUSTAINABLE SYSTEMS
www.advsustainsys.com

# Foldable and Recyclable Iontronic Cellulose Nanopaper for Low-Power Paper Electronics

*Inês Cunha,* Sofia Henriques Ferreira, Jorge Martins, Elvira Fortunato, Diana Gaspar, Rodrigo Martins, and Luís Pereira**

**An increase in the demand for the next generation of "Internet-of-Things" (IoT) has motivated efforts to develop flexible and affordable smart electronic systems, in line with sustainable development and carbon neutrality. Cellulose holds the potential to fulfil such demands as a low-cost green material due to its abundant and renewable nature and tunable properties. Here, a cellulose-based ionic conductive substrate compatible with printing techniques that combines the mechanical robustness, thermal resistance and surface smoothness of cellulose nanofibrils nanopaper with the high capacitance of a regenerated cellulose hydrogel electrolyte, is reported. Fully screen-printed electrolyte-gated transistors and universal logic gates are demonstrated using the engineered ionic conductive nanopaper and zinc oxide nanoplates as the semiconductor layer. The devices exhibit low-voltage operation (<3 V), and remarkable mechanical endurance under outward folding due to the combination of the robustness of the nanopaper and the compliance of the semiconductor layer provided by the ZnO nanoplates. The printed devices and the ion-conductive nanopaper can be efficiently recycled to fabricate new devices, which is compatible with the circular economy concept.**

## 1. Introduction

The unsustainable model used for developing electronic devices has led to an increase in the overharvesting of natural resources and electronic waste (E-waste) generation.[1,2] More abundant and renewable materials and simplified and economically efficient manufacturing processes, such as solution-phase printing techniques, are mandatory for fabricating new-concept systems that can be made massive and serve the IoT. The resulting devices and smart systems are also expected to have low-power consumption, capable of assuming different form factors and being compliant with mechanical deformations.[3]

One obvious option when considering sustainable smart systems is cellulose, the most abundant and renewable biopolymer resource on Earth.[4–6] Cellulose/paper is also compatible with roll-to-roll (R2R) manufacturing processes, enabling large-area applications at a reduced cost, and is available in several textures, compositions and coatings.[7,8] The reengineering of cellulose/paper with new functionalities allowed it to extend its application beyond the conventional ones, finding potential in electronics, photonics, energy and sensing.[1,8–13]

In 2008,[14] a new concept was introduced in exploring the hydrophilic network of the entangled cellulose fibers of paper that combines excellent mechanical and dielectric properties.[15] It was demonstrated that paper can be applied as a "dual-functional" layer (simultaneously as the substrate and solid-state electrolyte) in oxide semiconductor-based field-effect transistors (FETs),[14,16,17] write-erase and read memory transistors,[18] complementary metal-oxide-semiconductor (CMOS) devices,[19,20] logic gates,[3,21] and energy storage devices.[22–24]

Despite its unquestionable versatility and potential, the porosity and the large surface roughness of paper pose some obstacles to host electronic devices, especially when smoothness is a key criterion for reducing interfacial defects between active layers of transistors and achieving optimized electrical performance.[10,11] Additional coatings are usually required to achieve a smoother and less absorbent surface, which can further compromise coated paper's low-cost and recyclability/biodegradability.[11,25] The use of intrinsically smooth cellulose nanopaper substrates can address such problems.[16,17]

Furthermore, the operating voltage of the conventional paper-gated transistors and integrated circuits is still in the range of tens of volts to enable the formation of electric double layers (EDLs).[3,15] This hampers their application in IoT devices and systems, which require a maximum supply of a few volts to allow the use of portable power supplies, such as thin-film

I. Cunha, S. H. Ferreira, J. Martins, E. Fortunato, R. Martins, L. Pereira
CENIMAT|i3N
Department of Materials Science
School of Science and Technology
NOVA University Lisbon and CEMOP/UNINOVA
Campus da Caparica, Caparica 2829-516, Portugal
E-mail: i.cunha@campus.fct.unl.pt; lmnp@fct.unl.pt
D. Gaspar, L. Pereira
AlmaScience
Campus da Caparica, Caparica 2829-516, Portugal
The ORCID identification number(s) for the author(s) of this article can be found under https://doi.org/10.1002/adsu.202200177.



**DOI: 10.1002/adsu.202200177**

batteries.[10,26,27] One way to drastically reduce the operating voltage is by employing electrolytes with high specific capacitance (typically 1–10 μF $cm^{-2}$) as the gate dielectric.[28–30] Free-standing cellulose-based hydrogel electrolytes with excellent electrochemical properties, either prepared from ionic liquids[31] or aqueous alkali salt/urea solvent system,[32,33] have been reported in the literature. Though, the sticky, soft, and easily deformable surface is challenging to host a device.

In this context, we propose an all-cellulose ionic conductive composite (ACICC) membrane that combines the mechanical robustness and smoothness of micro/nanofibrillated cellulose nanopaper with appealing electrochemical properties of a regenerated cellulose hydrogel electrolyte prepared from the aqueous alkali salt/urea solvent system. As a result, we obtained a solid-state electrolyte in the form of a flexible sheet with a highly smooth and compact surface, reasonable transparency, and appealing electrochemical properties suitable for flexible/foldable electronics based on ionic responses (iontronics).

Screen printing was used to print nanopaper composite gated transistors (NCGTs), avoiding expensive conventional microfabrication techniques, such as sputtering and evaporation, which are commonly used in fabricating paper-gated transistors.[11,13,34] Inspired by the recent developments done in our research group in the field of printed oxide-based electronics on paper,[35–37] a screen-printable water-based ink composed of zinc oxide nanostructures was used to pattern the semiconductor layer of the transistors directly on the ACICC membrane. The adoption of planar configuration to further simplify the design of the transistors enables the fabrication of the first fully printed oxide-based NCGTs and integrated "universal" logic gates (NAND and NOR) with low-voltage operation, capable of withstanding extreme mechanical deformation under outward folding.

## 2. Results and Discussion

### 2.1. Characterization of the Iontronic Cellulose Nanopaper Composite

When considering the new paradigms of sustainable development and the growing environmental concerns related to E-waste and plastic pollution, cellulose becomes an increasingly attractive resource to be explored, which is in line with the 12th and 13th of the Sustainable Development Goals.[38] In addition to such interest, cellulose/paper as a solid-state dielectric substrate material in transistors has revolutionized electronic applications, where being low-cost, recyclability and flexibility are crucial.[3,14,16–21] Further advances in paper and cellulose engineering open an opportunity to explore strategies to lower the operating voltage of paper-gated transistors, which is a challenge to be overcome to meet the demands of IoT applications.

As demonstrated in our previous works,[32,33,35] high-capacitance cellulose-based ionic conductive hydrogels (CICHs), prepared by dissolving cellulose in an aqueous lithium hydroxide (LiOH)/urea solvent system, are promising ionic conductors for drastically reducing the transistors' operation voltage from tens of volts to just less than 3 V. However, these materials are not suitable to be used as substrates of electronic devices, since their hydrogel-nature makes them highly sensitive to environmental conditions, thus deforming the layers deposited on them.

To solve this issue, an ACICC membrane was developed by combining the advantages of the mechanical, optical, and thermal properties of cellulose nanopaper with the electrochemical properties of an ionic hydrogel. This new class of "paper-like" ionic conductive substrates is then obtained by slow casting and evaporation of water from an aqueous mixture of micro/nanofibrous cellulose pulp with the CICH slurry at room temperature conditions.

As shown in **Figure 1**b, the ACICC membrane (visible in Figure 1a) and the cellulose nanopaper possess high total optical transmittance in the visible region of the spectrum (400–800 nm), mostly above 80%, due to their micro/nanosized fibers that contribute to a denser structure, as verified by the SEM images (Figure 1c–e and Figure S1, Supporting Information). Still, differences in the optical and morphological properties can be observed in both membranes. In the case of the ACICC membrane, incorporating an ionic hydrogel in the nanopaper promotes the swelling of the narrow (≈20–90 nm range), tightly packed, and entangled hydrogen-bonded micro/nanofibrils. Some microfibrils are visible, reaching in some cases hundreds of nanometers in width and a length of several micrometers. The cross-sectional images reveal a unique layered porous network structure with a pore size of tens of nanometers. It is beneficial for relieving the mechanical stress induced in the functional layers deposited on its surface, contributing to its excellent flexibility.[39] In the ACICC membrane, the hydrogel fills the layered porous structure increasing its impermeability and transparency, promoting a shift of the total transmittance from 86% (cellulose nanopaper) to 88% (ACICC membrane) at 700 nm, making them suitable for transparent paper electronics.[39,40]

As confirmed by atomic force microscopy (AFM) measurements (Figure S2, Supporting Information), the ACICC membrane has a smoother and less permeable surface compared to cellulose nanopaper, showing a decrease in RMS roughness of nearly 11% (from 77 to 68 nm). The smoothness can be further improved by downsizing the fibril's dimension through combined mechanical, enzymatic, and/or chemical pre-treatment of cellulose fibers' pulp before mechanical shearing to obtain a nanocellulose pulp.[4] Dielectrics with smooth surfaces lead to fewer interfacial defects between the active layers of devices, making surface smoothness a key criterion for obtaining transistors and integrated circuits with better electrical performance.[11] Therefore, the smoothest surface of the ACICC membrane, corresponding to the side dried in contact with the container, is the one used to fabricate the iontronic devices.

In Figure S3a, Supporting Information, the XRD pattern of the CICH membrane exhibits two peaks at 20° and 22° for (110) and (200) planes, respectively, which are characteristic of a cellulose II crystal, thus confirming the regeneration of cellulose with acetic acid.[41] While the dissolution of cellulose destroys its crystallinity, the regeneration process with acetic acid exposes the hydroxyl groups of cellulose, inducing its self-aggregation to rapidly form physical hydrogels with new bonds, such as van der Waals, hydrophobic, and inter- and intramolecular hydrogen bonding.[42] On the other hand, the crystalline structure and respective crystalline index (CrI) of the ACICC membrane are

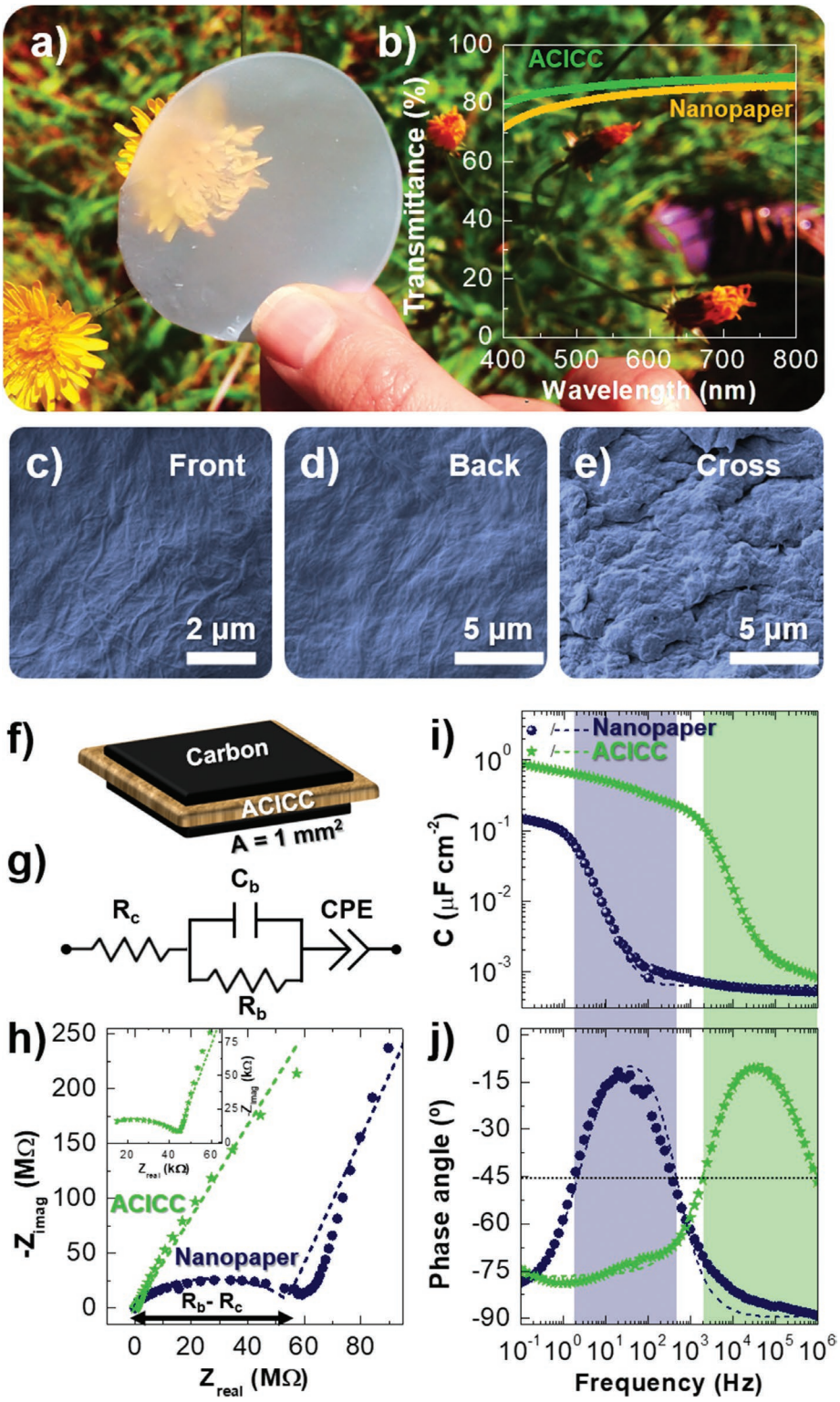


**Figure 1.** Characterization of the developed iontronic cellulose nanopaper composite. a) Photograph of the developed ACICC membrane, and b) its total transmittance compared with cellulose nanopaper. SEM micrograph images of ACICC membrane on distinct surfaces: c) front, d) back surfaces, and e) cross-section. f) Design of the electrochemical cell consisting of a typical capacitor structure (carbon/membrane/carbon) with an active area of 1 mm$^2$. g) Equivalent circuit model (ECM) used for data fitting, where $R_c$, $R_b$, $C_b$, and CPE correspond to contact resistance, bulk resistance, bulk capacitance, and constant phase element, respectively. h) Nyquist plots for the cellulose-based membranes and respective i) capacitance and j) phase angle as a function of frequency, where the ionic relaxation region is highlighted in blue and green for the cellulose nanopaper and ACICC membrane, respectively. The symbols and the dashed lines denote the experimental and the fitted data, respectively.

not affected by the addition of the regenerated cellulose-based slurry into the micro/nanocellulose pulp. The characteristic peaks for ($1\bar{1}0$), (110) and (002) crystallographic planes at $2\theta$ = 14.3°, 16.3° and 22.4°, respectively, correspond to cellulose I.[43]

According to the empiric method proposed by Segal et al.,[44] the CrI was calculated using Equation S1, Supporting Information, estimated to be ≈61% and ≈65% for ACICC and cellulose nanopaper, respectively. It is noteworthy that the values estimated for the CrI of both nanopaper-based membranes are only useful to compare their relative differences, as the CrI differs significantly depending on the technique and calculation method adopted.[17,45]

We also evaluated the amount of water retained within the cellulose-based membranes by FTIR (Figure S3b, Supporting Information). The spectra were baseline corrected to 0 at 1845 and 3739 $cm^{-1}$ and normalized to 1 at 2900 $cm^{-1}$, forming a common baseline for the qualitative study of the water content in the membranes.[46] The FTIR spectra of cellulose nanopaper and ACICC membrane reveal a series of characteristic absorption bands for cellulose at 3600–3000, 2900 and 1635 $cm^{-1}$, which are assigned for stretching vibration of H-bonded O—H groups, C—H stretching and O—H bending of adsorbed water, respectively.[47] Typical bands assigned to cellulose at 1160 and 894 $cm^{-1}$ are due to C—O—C stretching vibrations of the $\beta(1\rightarrow4)$-glycosidic links in cellulose.[48,49] The absorbance at nearly 1051 and 1028 $cm^{-1}$ is attributed to C—O—C pyranose ring skeletal vibrations.[49] Some additional bands are visible in the ACICC membrane due to the contribution of urea hydrates and regenerated cellulose from the hydrogel electrolyte. The bands in the region between 1750 and 1520 $cm^{-1}$ can be related to Amide I and Amide II of urea molecules. In contrast, the small shoulder band at 3448 $cm^{-1}$ corresponds to a characteristic band of cellulose II, assigned to O—H groups forming intramolecular hydrogen bonds.[48]

The evolution of water retention can be compared by looking closer to the broad band at 3600–3000 and 1635 $cm^{-1}$.[17] These bands are more pronounced in the CICH membrane than in the cellulose nanopaper, as it possesses abundant charged hydrophilic functional groups and alkali metal ionic species that promote better water retention within the regenerated cellulose network. The addition of the cellulose-based hydrogel to the micro/nanofibrous material increases water retention, showing a behavior between the CICH membrane and the cellulose nanopaper.

Figure S3c, Supporting Information, shows the thermal degradation of the individual materials that compose the engineered nanopaper composite. According to the weight loss curves, the ACICC membrane exhibits intermediate thermal stability between the CICH membrane and cellulose nanopaper, confirming its "composite" character. The thermal degradation of the ACICC membrane occurs in two steps, starting with the desorption of moisture adsorbed in the cellulose matrix at temperatures below 100 °C, followed by a steep weight loss up to 295 °C related to the thermal degradation of the material. The thermogravimetric analysis (TGA) also confirms that the CICH has a more pronounced weight loss in the first stage (≈11% at 100 °C) compared to the nanopaper (≈3.9% at 100 °C) and ACICC membrane (≈6.6% at 100 °C), as its hydrogel character enables the presence of a higher amount of weakly bound water that is adsorbed in the cellulose network.

Considering these results, which are in line with the FTIR results, the ACICC membrane combines the thermal resistance of micro/nanofibrillated cellulose nanopaper with the superior water adsorption ability of the CICH membrane. The latter feature has a tremendous impact in the electrochemical properties, which were also studied in this work.

The electrochemical characterization of the cellulose nanopaper and the developed ACICC membrane was carried out under ambient conditions, using a typical capacitor structure, where carbon electrodes were screen-printed on both sides of the membranes with an area of 1 $mm^2$ (Figure 1f). Figures 1i,j show the measured specific capacitance ($C$) and phase angle ($\theta$) as a function of frequency in the range of 0.1 Hz to 1 MHz, and the respective Nyquist plot is shown in Figure 1h.

Distinct polarization mechanics occur depending on the range of frequencies under consideration and the "degree" of ionic enrichment of the membranes. For the nanopaper, three regimes can be distinguished, starting with the dipole relaxation that occurs for higher frequencies (≈0.5 kHz to 1 MHz, $\theta < -45°$), moving sequentially to ionic relaxation (2 Hz to 0.5 kHz, $\theta > -45°$, highlighted in blue in the plot), related to a dominant resistive behavior, and then a transition to a prevailing capacitive regime occurs as frequency decreases (<2 Hz, $\theta < -45°$), due to the EDL formation. In the last regime, the mobile ionic species trapped within the nanopaper matrix, which are mainly responsible for protonic conduction (the Grotthuss mechanism),[50] migration toward the nanopaper/carbon interfaces. This migration promotes an abrupt increase in the capacitance to 0.15 μF $cm^{-2}$ at 0.1 Hz, whilst the phase angle approaches −80°, as the nanopaper does not behave as a purely capacitive element. These results are in agreement with other works in the field of paper electronics,[17,50] which propose that the water sorption mechanism promotes the formation of the EDL in cellulose-based nanomaterials, providing protons and hydroxyls that are responsible for the ionic conduction and build-up of the capacitance at low frequencies.

The ionic performance is considerably improved when mixing the micro/nanocellulose pulp with a small amount of the hydrogel electrolyte enriched with hydrated alkali metal ionic species, as it aids in water retention within the membrane matrix, as demonstrated previously by FTIR and TGA measurements. The EDL formation occurs for higher frequencies (<2 kHz), reaching a maximum capacitance close to 1 μF $cm^{-2}$ at 0.1 Hz, where the phase angle levels around −75° due to a non-ideal capacitive behavior. The Nyquist plot of the ACICC membrane reveals a shrinkage of the semicircle width, corresponding to the difference between the bulk and contact resistances ($R_b$ and $R_c$, respectively, as indicated in the plot), which suggests an apparent enhancement of both capacitance and ionic conductivity ($\sigma_i$) in comparison to nanopaper.

A reasonably good fitting is obtained to the data by using the equivalent circuit model (ECM) depicted in Figure 1g, containing a $R_c$ in series with a RC circuit (related to the $R_b$ and bulk capacitance, $C_b$) and a constant phase element (CPE). The proposed ECM was used to determine the $\sigma_i$ of both membranes, which was estimated from five samples using Equation S2, Supporting Information. The cellulose nanopaper yields a low $\sigma_i$ value ≈$(9.38 \pm 0.88) \times 10^{-9}$ S $cm^{-1}$,

which is increased by more than three orders of magnitude to $(4.18 \pm 0.36) \times 10^{-5}$ S cm$^{-1}$ for the ACICC membrane.

Regarding the electrochemical stability of the engineered nanopapers, there is no evidence of redox peaks in the cyclic voltammetry (CV) measurements in the voltage range between −2.5 and 2.5 V at a fixed scan rate of 0.2 V s$^{-1}$, which are the same parameters used in the NCGTs' characterization (Figure S4a, Supporting Information). The ACICC membrane exhibits superior current values compared to nanopaper, yet the currents observed for both membranes are mainly related to the double layer charging.

The possibility of electrochemical reactions between the electrolyte and the oxide semiconductor should not be disregarded, which will ultimately influence the operation mode

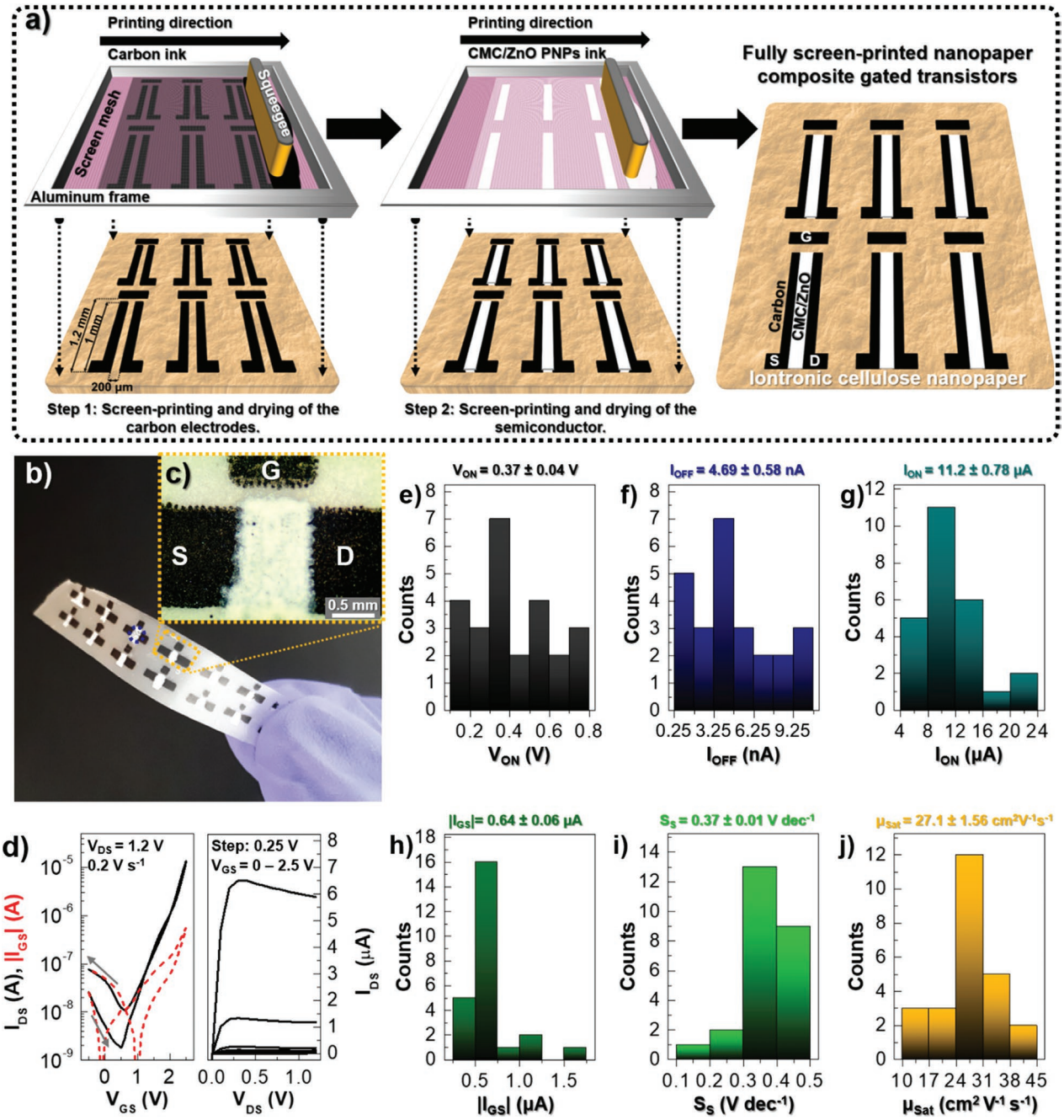


**Figure 2.** Design and electrical characterization of the fabricated fully screen-printed ZnO NCGTs. a) Schematic illustration of the fabrication process of the NCGTs. b) Photograph of the fabricated EGTs on the ACICC membrane. c) Optical micrograph image of a single NCGT (S, G and D stand for source, gate and drain electrodes). d) Transfer characteristic curve ($I_{DS}$–$V_{GS}$) and respective output curve ($I_{DS}$–$V_{DS}$, the step for the $V_{GS}$ was 0.25 V, from −0.5 to 2.5 V) collected with a $V_{GS}$ scan rate of 0.2 V s$^{-1}$. Arrows represent the sweep direction, whereas continuous and dashed lines correspond to $I_{DS}$ and $|I_{GS}|$, respectively. Histograms of device metrics for 25 devices, including the e) turn-on voltage ($V_{ON}$), f) OFF current ($I_{OFF}$), g) ON current ($I_{ON}$), h) gate leakage current ($|I_{GS}|$), i) subthreshold gate voltage swing ($S_S$), and j) saturation mobility ($\mu_{Sat}$).

of the NCGTs as well as their switching speed. Therefore, the electrochemical stability of the carbon/ACICC/semiconductor/carbon layered structure, which simulates the structure of the printed ZnO NCGTs displayed in **Figure 2**a, was also evaluated (Figure S4b, Supporting Information). The interface between the electrolyte and the semiconductor leads to the appearance of redox peaks that can evidence the permeability of the semiconductor to ions existent within the ACICC membrane. Therefore, we can predict a mixed operating mode mechanism (field-effect and electrochemical doping).

In conclusion, the ACICC membrane combines a unique set of features from a smooth surface, semi-transparency and temperature resistance to good electrochemical properties, which lead us to explore its full potential as an ionic conductive substrate in low-voltage NCGTs and logic gates.

### 2.2. Design of the Nanopaper Composite Gated Transistors

Screen printing is widely used in printed electronics,[11,51,52] being scalable to the industrial level and suitable for high-volume R2R fabrication.[51] Considering the several advantages offered by this printing technique, fully screen-printed planar ZnO NCGTs with a channel length ($L$) and width ($W$) of 200 and 1000 μm ($W/L \approx 5$), respectively, were fabricated on the smoothest side of the ACICC membrane (Figures 2a–c).

Only two printing steps are needed to fabricate fully functional NCGTs by patterning the planar carbon electrodes (sheet resistance - $R_s = 253 \pm 10.2\ \Omega\ \square^{-1}$, determined from four-point probe measurements using Equation S3, Supporting Information), and then the semiconductor layer onto the ACICC. The planar architecture reduces the mechanical stress applied to the device compared to the vertical structure. It simplifies device fabrication since it minimizes deposition steps and reduces the need for complex alignment procedures.

In our previous work,[35] we demonstrated screen-printed ZnO electrolyte-gated transistors (EGTs) and logic gates. A screen-printable composite semiconducting ink composed of small-sized (<200 nm) commercial ZnO nanoparticles (NPs) was formulated for such purpose. A water-soluble cellulose derivative, sodium carboxymethyl cellulose (CMC), was used as a thickening, rheological and dispersing agent to provide thixotropic behavior and good dispersion and stability of the ZnO NPs, ensuring mechanical robustness and adhesion to the office paper substrate. Although its water-based formulation is desirable, a high loading content of functional material (40 wt%) is needed to achieve electrical percolation and current modulation in the fabricated screen-printed EGTs and circuits. Despite the mechanical flexibility under bending demonstrated by such devices, the thick channel layer is damaged under folding.

The percolative pathways for conduction can be improved by using particles with a higher aspect ratio, while enhancing the mechanical endurance of the functional layer.[31,53] Therefore, porous ZnO nanoplates (ZnO PNPs) were used as an alternative to commercial ZnO NPs. Interestingly, there are several reports demonstrating the superior performance of ZnO PNPs in gas sensors, ultraviolet sensors, dye-sensitized solar cells, nanogenerators, photocatalysis, and biosensing. Yet, their performance in transistors and circuits has never been tested.[36,54–56]

Figure 2b,c shows an optical micrograph image of the functional layers printed on the ACICC membrane. Close examination of the SEM images in Figure S5, Supporting Information, reveals a semiconductor layer with a dense and compact network structure of randomly oriented stacked ZnO PNPs, showing no signs of cracking along its surface or peeling. The particles are thin (<100 nm thickness), elongated (maximum length: <3.5 μm) and exhibit serrated edges, as well as a highly porous surface with a pore size in the range of hundreds of nanometers that is formed during the calcination step at 700 °C. The nanoplate-shape provides a more direct percolation path for electron transport and a larger interface between the particles and the ACICC substrate. Some bundles, aggregates and voids are visible, responsible for the slightly rough and irregular surface. The contact between the ZnO PNPs could be further improved by combining ZnO particles of smaller size or coating their surface with zinc precursor solution.[21,53]

### 2.3. Characterization of the Nanopaper Composite Gated Transistors

Figure 2d shows typical cyclic transfer (drain current $I_{DS}$ versus gate voltage $V_{GS}$) and respective output ($I_{DS}$ versus drain voltage $V_{DS}$) curves of the fabricated fully screen-printed ZnO NCGTs. The devices were tested 1 h after printing de semiconductor layer under ambient conditions (≈40% RH). Statistical variations of twenty-five devices are displayed in the histograms of Figures 2e–j, corresponding to the vital figure of merits of transistors, which strongly depend on the capacitance of ACICC membrane and its surface defects. The electrical parameters, such as turn-on voltage ($V_{ON}$), ON ($I_{ON}$) and OFF ($I_{OFF}$) currents, respective ON/OFF current ratio ($I_{ON/OFF}$), gate leakage current ($I_{GS}$), subthreshold gate voltage swing ($S_S$) and saturation mobility ($\mu_{Sat}$), were calculated in the forward sweep direction and in the saturation regime ($V_{DS}$ = 1.2 V). The corresponding mean values and their standard error of the mean are also mentioned.

The $S_S$ and $\mu_{Sat}$ were calculated according to Equations S4 and S5, Supporting Information, respectively. To avoid overestimation of the NCGTs' mobility the value used for the capacitance of the ACICC membrane was the one obtained at the lowest value of frequency (0.1 Hz), within the EDL formation regime, from electrochemical impedance spectroscopy (EIS) measurements, which corresponds to ≈0.8 μF cm$^{-2}$.

The fabricated NCGTs operate with negligible hysteresis (anti-clockwise direction) in enhancement mode with a $V_{GS}$ of less than 2.5 V, which is much lower than conventional cellulose-based paper transistors, typically reported on the order of tens of volts. The noticeable decrease in operation voltage is due to the high lateral capacitive coupling effect induced by the ionic conductivity of the ACICC membrane. The mobile ions can respond laterally to a transverse electric field and accumulate at the gate/electrolyte and semiconductor/electrolyte interfaces, depending on the $V_{GS}$ value. By doing so, the channel conductance varies by more than three orders of magnitude ($3.5 \times 10^3$), reaching an $I_{OFF}$, $I_{ON}$ and $|I_{GS}|$ of 4.69 ± 0.58 nA, 11.2 ± 0.78 μA and 0.64 ± 0.06 μA, respectively.

The large $|I_{GS}|$ observed is closely related to the faradaic redox currents (as previously confirmed by CV measurements

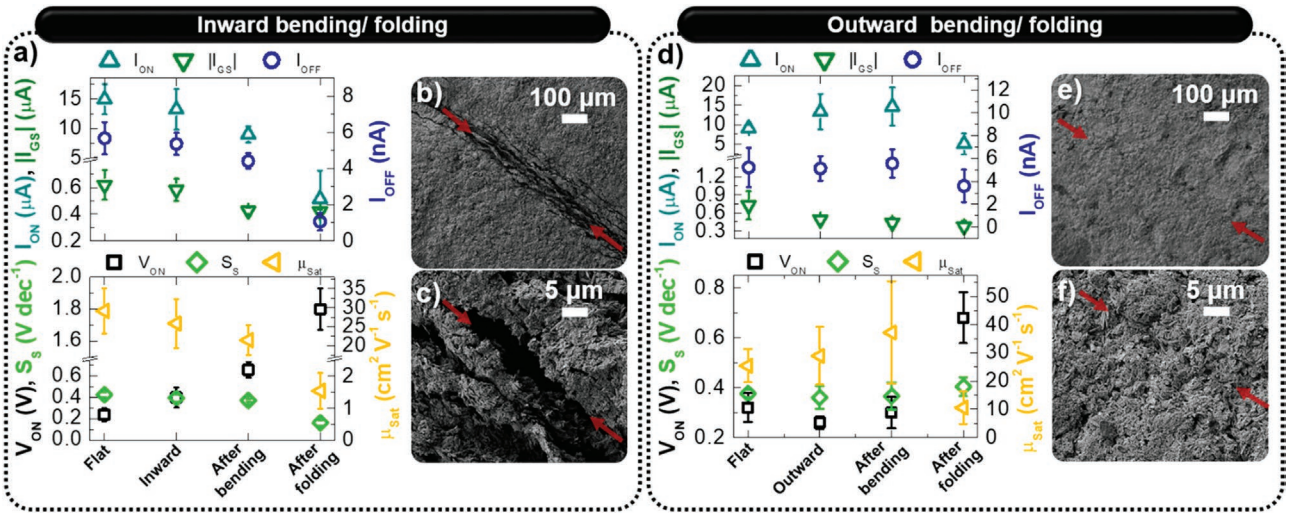


**Figure 3.** Electrical characterization of the fabricated fully screen-printed ZnO NCGTs before and after inducing mechanical deformation. Variation of the electrical parameters before and after performing a) inward or d) outward bending/folding ($V_{DS}$ = 1.2 V, $V_{GS}$ scan rate = 0.2 V $s^{-1}$). The data points show the average and corresponding errors bars obtained from five samples. SEM images of the devices in the flat state after performing (b,c) inward or (e,f) outward folding.

in Figure S4b, Supporting Information), since small ions, such as protons and lithium ions, tend to diffuse into the highly permeable semiconductor layer. Its porous morphology works as electrochemically active sites that promote electrochemical reactions, inducing a 3D conduction channel. Both $I_{DS}$ and $|I_{GS}|$ curves exhibit distinct behaviors depending on the applied $V_{GS}$. This evidences that a different operation mechanism becomes dominant, shifting from a field-effect to a predominant electrochemical doping regime for higher $V_{GS}$ values. Furthermore, the devices exhibit a large $\mu_{Sat}$ of 27.1 ± 1.56 $cm^2$ $V^{-1}$ $s^{-1}$, and a relatively small $S_S$ of 0.37 ± 0.01 V $dec^{-1}$. According to the output characteristics, the printed devices show hard saturation behavior at very low $V_{GS}$ (<2.5 V) and $V_{DS}$ (<0.5 V).

We also examined the environmental stability of six printed ZnO NCGTs over time, whose transfer curves are measured at as-prepared conditions and after three weeks (Figure S6, Supporting Information). Their electrical performance is quickly degraded after a few days, decreasing the electrical modulation by almost one order of magnitude, while $\mu_{Sat}$ decays by 95%. The devices no longer exhibit satisfactory electrical modulation for storage periods longer than a week since the $|I_{GS}|$ surpasses the $I_{ON}$. A possible explanation lies in the reactivity of ZnO nanostructures with protons and hydroxyl ions from the electrolyte, leading to the formation of zinc complexes under potential biases and/or UV light illumination.[57–59] Since the performance is not maintained for long periods, they are best suited for disposable applications.

Furthermore, devices should withstand mechanical deformations without degrading their performance. Although several reports have demonstrated the flexibility of oxide-based paper transistors with proper operation under bending strains,[17,31,32,60,61] foldability has not been achieved. So far, organic semiconductors have shown superior endurance to mechanical deformation.[62]

**Figure 3**a,d show the variations in electrical performance of five devices before and after inducing a bending deformation along the channel axis, using a substrate holder with a bending radius of 15 mm, as well as the recovery to the flat state of the folded devices (see the respective transfer characteristic curves in Figure S7, Supporting Information). The ACICC membrane and the printed carbon electrodes show mechanical robustness after bending or folding, suggesting that the differences observed can be mainly attributed to the cracking, peeling or even alignment of the ZnO PNPs, depending on the type of induced mechanical deformation.

For inward bending, equivalent to inducing a compressive strain, there is a deterioration in the electrical properties, where a slight shift of $V_{ON}$ to higher values is observed, while $I_{ON}$ and $\mu_{Sat}$ reduce ≈12% and ≈11%, respectively, compared to its original performance in the flat state. These changes are due to the formation of some cracks/voids along the thick CMC/ZnO layer. Returning to the flat state, the performance is further degraded due to the peeling of crashed particles. Despite the propagation of the fractures in the channel layer during folding, the elongated size of the ZnO particles proves to be advantageous to guarantee enough percolation paths that ultimately avoid total failure of the devices after folding, as confirmed by SEM (Figure 3b,c).

A quite different behavior is observed when inducing a tensile strain. In this case, a considerable improvement in the devices' performance is observed, since the outward bending promotes the local preferential orientation of the particles in the source–drain direction, which facilitates electron transport, thus enhancing ion percolation within the ACICC membrane. These reasons explain the favorable increase of 47% and 14% of $I_{ON}$ and $\mu_{Sat}$, respectively, resulting in a 4% $I_{ON/OFF}$ optimization. Returning to the flat state promotes better accommodation of the locally oriented particles, restoring and creating new percolation paths, which in turn leads to further improving the NCGTs' performance. Comparing the performance before and after bending, $I_{ON}$ increases by 61%, whilst a 46% increase is achieved for $\mu_{Sat}$.

Regarding recovery after folding, the devices demonstrate a remarkable performance, showing a slight shift in $V_{ON}$ from

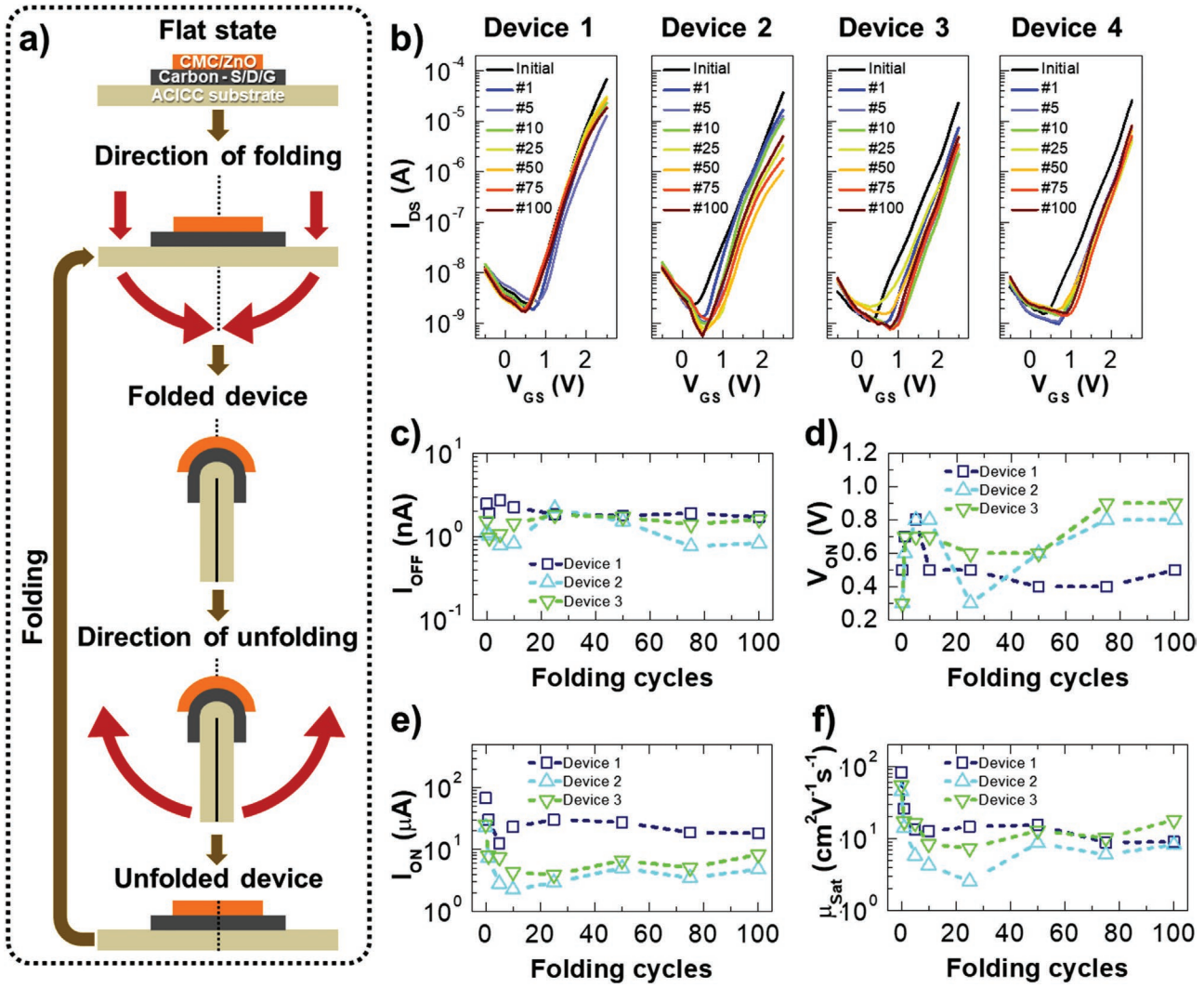


**Figure 4.** Mechanical electrical stress measurements of the fully screen-printed ZnO NCGTs on the flat state after consecutive 100 outward folding/unfolding cycles. a) Schematic representation of successive folding/unfolding cycles ($V_{DS}$ = 1.2 V, $V_{GS}$ scan rate = 0.2 V $s^{-1}$). b) $I_{DS}$–$V_{GS}$ curves of three devices after successive folding/unfolding cycles, and respective evolution of the electrical parameters: c) $I_{OFF}$, d) $I_{ON}$, e) $V_{ON}$, and f) $\mu_{Sat}$.

0.3 to 0.7 V, and a decrease in $I_{ON/OFF}$ of 24%. As observed in Figure 3e,f, the device remains unharmed after folding, which demonstrates a good semiconductor/ACICC membrane interface.

As depicted in **Figure 4**, the folding stability of three screen-printed ZnO NCGTs was assessed over 100 outward folding/unfolding cycles. The most significant changes occur during the first five cycles in a similar way as described above, showing a decrease in $I_{ON}$ and mobility and a shift in $V_{ON}$ to higher values. Their performance remains stable with increasing folding/unfolding cycles, which demonstrates that these devices have satisfactory mechanical tolerance, serving the purpose of flexible electronics.

Considering the current state-of-the-art in the field of cellulose (nano)paper-gated transistors (see Table S1, Supporting Information), this work's reports pioneer on fully printed transistors, where a "paper-like" ionic conductive membrane is successfully used as gate dielectric and substrate, while yielding devices with appealing electrical characteristics at low operating voltages and exceptional performance under folding. Considering such a fabrication strategy, the use of low-temperature (<100 °C) printing techniques in combination with simpler designs (planar configuration and "dual-functionality" of ACICC substrate) is highly appealing for large-scale production at extremely low-cost.

Dynamic measurements were performed to assess the electrical stress of the screen-printed ZnO NCGTs by applying a square-wave gate signal at different frequencies (**Figure 5**). The devices show an electrical modulation above two orders of magnitude at 0.1 Hz, and a steep decrease in $I_{ON/OFF}$ toward one order of magnitude is observed for frequencies between 5 and 10 Hz, the maximum frequency at which the fabricated logic gates are expected to operate. Although it is still possible to distinguish between the OFF and ON states at 25 Hz, the $I_{ON/OFF}$ does not reach one order of magnitude. Despite the ionic response of the ACICC membrane pointing to a capacitive behavior for superior frequencies (≈1.9 kHz), the large channel dimensions limit the devices' electrical switching.

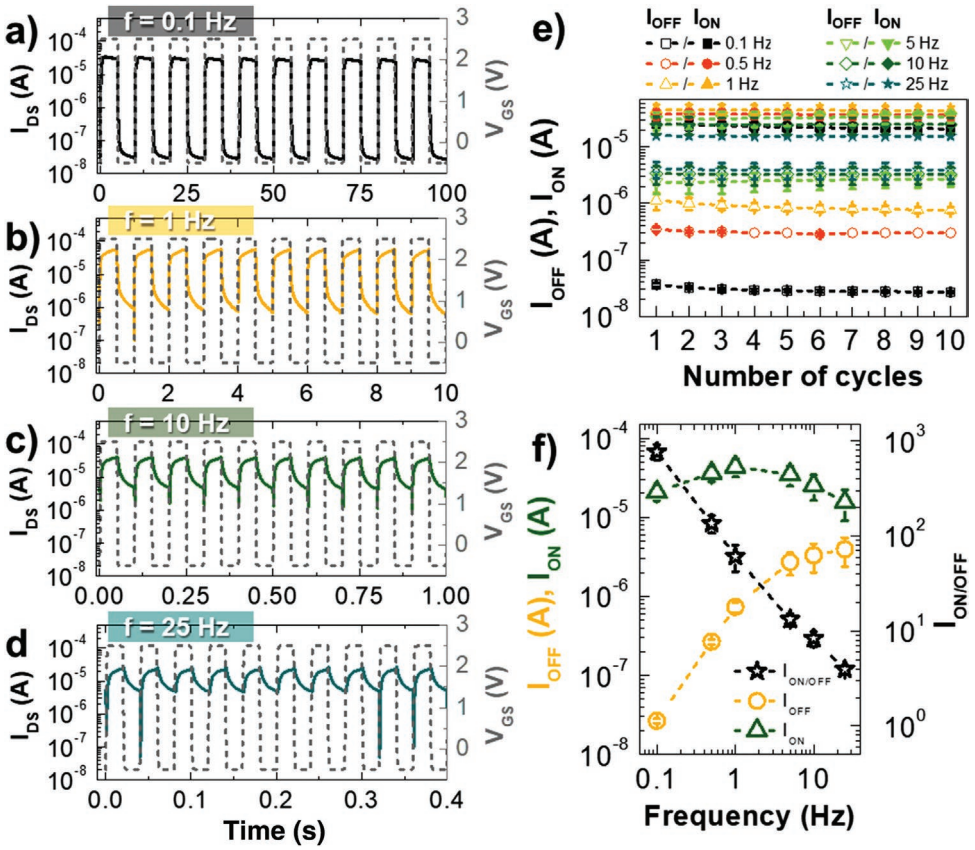


**Figure 5.** Dynamic electrical characterization of the fabricated fully screen-printed ZnO NCGTs. Variation of $I_{DS}$ with increasing cycles of $V_{GS}$ pulses from –0.5 until 2.5 V for different frequencies: a) 0.1, b) 1, c) 10, and d) 25 Hz. e) Variation of $I_{ON}$ and $I_{OFF}$ with increasing cycles for a square-wave gate signal between –0.5 until 2.5 V for a fixed $V_{DS}$ of 1.2 V and at different frequencies: (open symbols correspond to $I_{ON}$, while closed symbols correspond to $I_{OFF}$). f) Evolution of $I_{ON}$, $I_{OFF}$, and $I_{ON/OFF}$ with frequency for the tenth cycle (the data points show the average and corresponding errors bars obtained from three devices).

### 2.4. Characterization of the Nanopaper Composite Logic Gates

These devices were integrated into digital logic circuits to develop further applications based on the fabricated planar, fully screen-printed ZnO NCGTs (**Figure 6**a). An example is the logic inverter (or NOT gate), the basic building block in digital electronics, able to invert an input signal. An inverter is constructed by connecting a load resistance ($R_L$) to a drive transistor ($EGT_D$). More complex logic gates, such as NAND and NOR gates, can be successfully fabricated by connecting two transistors ($EGT_A$ and $EGT_B$) and a pencil-drawn $R_L$. While in the NAND gate the two transistors are in series, the NOR gate consists of two transistors in parallel.

A pencil was used to pattern resistive graphitic tracks that establish the $R_L$. A sheet of office paper was used instead of the ACICC membrane as its naturally rough surface easily exfoliates the graphite particles through mechanical abrasion of the pencil toward the paper.[63] The ACICC membrane was glued to the office paper with double-sided tape, and the transistors were printed on its smooth surface. After printing the carbon electrodes, a brush was used for handwriting thick carbon conductive tracks. The drawn electrical connections and the screen-printed electrodes were dried at 70 °C for 15 min, and stored at ambient conditions for 1 h to allow the ACICC membrane to restore its moisture level before printing the CMC/ZnO channel. This way, it is possible to easily bridge the intended electrodes of the hosting cellulose-based materials (office paper and ACICC membrane).

Figure 6b shows the voltage transfer characteristic (VTC) curves of the NOT gate with a pencil-drawn $R_L$ of 300 kΩ and an $EGT_D$ with L = 200 µm and W = 1 mm. The circuit shows a clear steep inversion behavior with low output hysteresis when $V_{IN}$ is swept from –0.5 V (logic input signal "0") to 3 V (logic input signal "1") for a low $V_{DD}$ of 1.5 V. The $V_{OUT}$ at logic input signal "0" is close to the $V_{DD}$ (≈1.43 V), which is determined by $V_{OUT} = V_{DD} - R_L \times I_{DS}$. When the transistor switches to the ON state with increasing $V_{IN}$, $V_{OUT}$ drops almost to zero (≈ 0.05 V), and the inverter exhibits a maximum |gain| ($-\partial V_{OUT}/\partial V_{IN}$) of 2.9.

The output characteristics of the NAND and NOR logic gates are shown in Figure 6c and 6d, respectively, also showing low hysteresis. In the case of the NAND gate, when one or both of the input gate voltages ($V_{IN,A}$ and $V_{IN,B}$) are logic "0" ($V_{IN,A} = 0$ or $V_{IN,B} = 0$ V), the $V_{OUT}$ is "HIGH" (1.34 V), corresponding to output logic "1". Only when both input gate voltages are logic "1" ($V_{IN,A} = V_{IN,B} = 3$ V), the transistors turn to the ON state and the $V_{OUT}$ becomes "LOW", corresponding to output logic "0" (0.09 V), reaching a |gain| of 1.6.

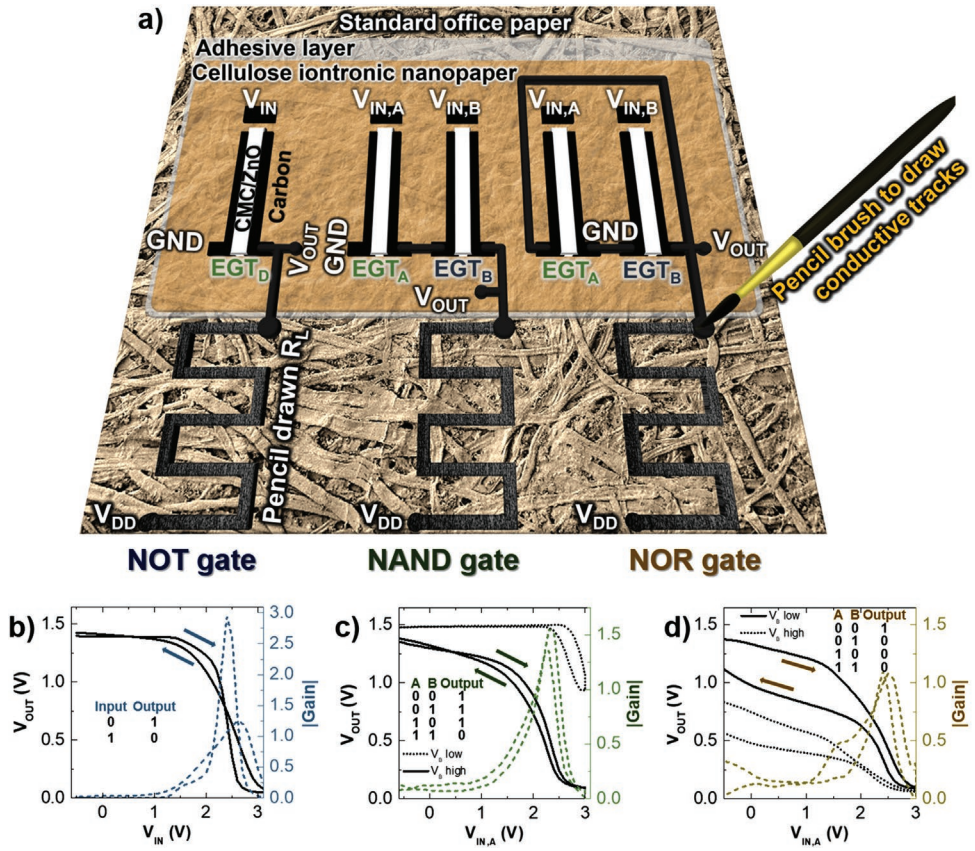


**Figure 6.** Logic gate applications of the planar fully screen-printed ZnO NCGTs with pencil-drawn load resistances. a) Schematics of the fabricated logic gates (NOT, NAND, and NOR gates): the ACICC membrane that hosts the screen-printed ZnO NCGTs is glued to a sheet of standard office paper, where are pencil-drawn different graphitic load resistances with 300 kΩ, and thick carbon conductive tracks are painted with a pencil brush to establish the proper electrical connections between the individual transistors from the ionic conductive substrate and the respective $R_L$ deposited on office paper. VTC curves of b) the NOT gate; c) NAND gate, and d) NOR gate, and respective |gain| for $V_{DD}$ = 1.5 V at a fixed voltage sweep rate of 0.2 V $s^{-1}$. Truth tables of the fabricated logic gates are summarized as insets in the respective plots.

In contrast, for the NOR gate, the output signal "1" is obtained only when all the transistors are in the OFF state. The maximum value to set the output signal "1" corresponds to 1.33 V, reaching a |gain| of 1.1. The output logical "0" can be set by applying the input signals $V_{IN,A}$ = 3 V and $V_{IN,B}$ = 0 V, reaching a minimum value for $V_{OUT}$ of 0.09 V. Nevertheless, $V_{OUT}$ is slightly high when applying $V_{IN,B}$ = 3 V and low input signals $V_{IN,A}$, since either the $EGT_A$ is not entirely in the OFF state or $|I_{GS}|$ increased. In this case, when $V_{IN,B}$ = 3 V and $V_{IN,A}$ = 0 V, the $V_{OUT}$ records a value of 0.83 V.

The successful demonstration of low-voltage logic operations, from a simple resistor-loaded inverter to "universal" logic gates, represents an important step for portable paper electronics, since thin-film batteries or energy harvesting schemes can power such circuits.[64]

### 2.5. Biodegradability/Recycling Assessment

Although the use of cellulose-based paper substrates in electronics is usually linked to disposable devices due to their biodegradable nature,[65] recycling is preferable to avoid producing waste in landfills.[13,32,33,66,67] Considering the short lifespan of the fabricated screen-printed ZnO NCGTs, we explored a non-toxic and low-cost process to recycle the devices (**Figure 7**a) efficiently.

Taking advantage of the water-based formulation of both electrolyte and semiconductor layers, the pristine ACICC membranes that host the iontronic devices were soaked in water, and then stirred to obtain a homogeneous pulp of fibers. The pulp was used as raw material for preparing recycled membranes by performing solvent-casting in polystyrene Petri dishes (see Video S1, Supporting Information). During stirring, the array of transistors disintegrates into individual devices and then gradually disappears, depending on the dispersion or dissolution rate of the various constituent materials.[68] As observed in previous reports,[69–71] ZnO can be easily dispersed in water. On the other hand, the carbon material from the electrodes and conductive lines has different dimensions and is randomly dispersed in the composite pulp, which can be partially sieved before preparing the recycled membrane.

The clear biodegradability of ACICC membrane and CMC/ZnO layer arises from concepts such as biodegradable electronics (or "transient electronics"), in which the materials completely or partially dissolve, resorb or physically disappear after functioning in environmental or physiological conditions at controlled rates.[71] Therefore, such devices can be used as

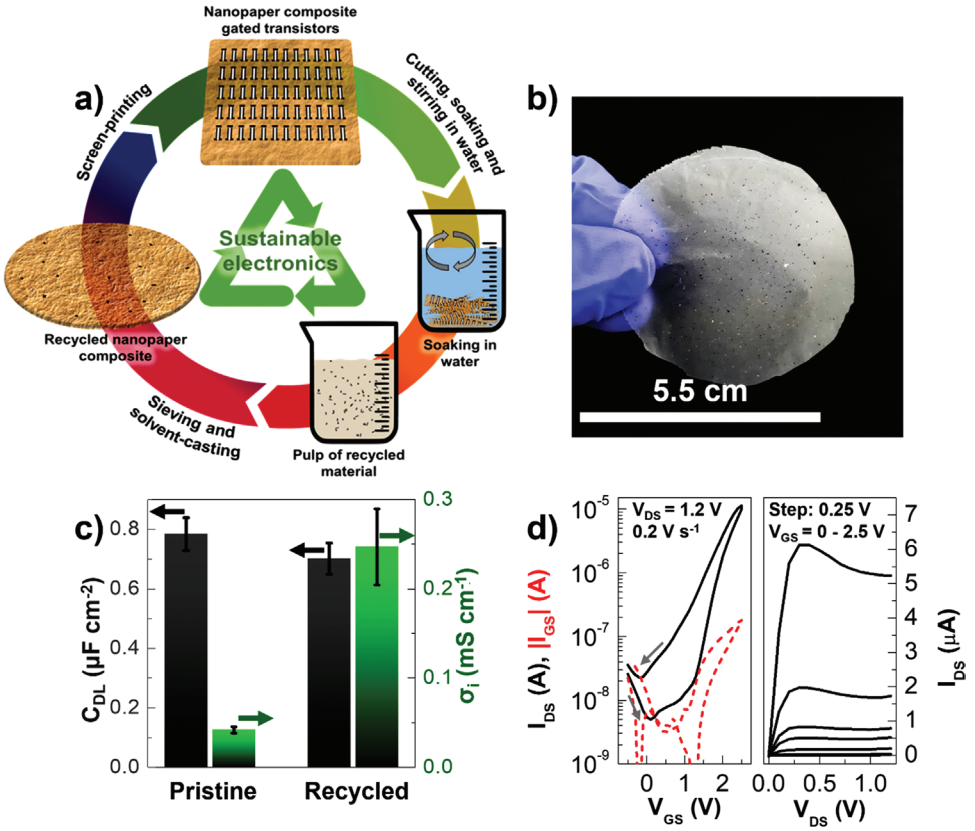


**Figure 7.** Characterization of the recycled ACICC membrane and electrical performance of screen-printed ZnO transistors fabricated on the recycled membrane. a) Circular economy loop for ACICC membrane using recycling strategies. b) Photograph of the recycled ACICC membrane. c) Comparison of capacitance and $\sigma_i$ for the pristine and recycled ACICC membranes. The data points show the average and corresponding errors bars obtained from five samples. d) $I_{DS}$–$V_{GS}$ curve and respective $I_{DS}$–$V_{DS}$ curve (the step for the $V_{GS}$ was 0.25 V, from −0.5 to 2.5 V), collected with a $V_{GS}$ scan rate of 0.2 V s$^{-1}$. Arrows represent the sweep direction, whereas continuous and dashed lines correspond to $I_{DS}$ and $|I_{GS}|$, respectively.

environmentally friendly alternatives to existing electronics that disintegrate when exposed to water, thus solving the problem of E-waste management.

Also, the composite pulp can be of greater use when recycled. Figure 7b shows a photograph of the resulting recycled ACICC membrane, which is less transparent and more fragile than the pristine one due to the presence of conductive carbon material and ZnO particles from the devices, as demonstrated by energy dispersive X-ray spectrometer (EDS) (Figure S8d, Supporting Information). Although sieving the carbon material minimizes the creation of irregularities on the surface, the recycled membrane still exhibits a quite irregular fibrous surface covered with waste material from the recycled devices (Figure S8a–c, Supporting Information). Thus, its surface is rougher than the pristine one, reaching a RMS roughness in a few hundred nanometers (Figure S8e, Supporting Information).

The electrochemical behavior is also very distinct compared to the pristine membrane (Figure S9, Supporting Information). Beyond the existing ionic species in the ACICC membrane, we need to consider the additional contribution of carbon and porous ZnO particles trapped within the membrane, as they create new interfaces. In particular, the ZnO particles exhibit high surface reactivity, due to their large active surface area and porous morphology filled with electrolytic species, working as electrochemically active sites where EDLs is formed and electrochemical reactions take place. These observations led us to the proposed ECM depicted in Figure S9a, Supporting Information, which produced a good fitting to the experimental data. This ECM has already been reported in the literature.[72]

As shown in Figure 7c, although the capacitance of the recycled membrane is slightly lower compared to the pristine one, the $\sigma_i$ and the maximum frequency at which the EDL formation occurs are substantially higher, reaching average values of the order of 15 kHz and 0.25 mS cm$^{-1}$, respectively. The incorporation of inorganic fillers, such as ZnO particles, into gel electrolytes has been reported as a promising way to enhance the ionic conductivity by developing additional conductive pathways.[73]

CV measurements reveal redox reaction peaks in the same range of voltages applied to operate the transistors printed on the recycled membrane under study, meaning that the devices can operate in mixed operating mode (field-effect and electrochemical doping mode) (Figure S9d, Supporting Information).

The recycled ACICC membrane was successfully reused as gate dielectric in printed ZnO transistors, working at low voltages with higher hysteresis and slightly lower performance compared to the pristine one (Figure 7d). The large counterclockwise current hysteresis behavior indicates the existence of a memory effect, being capable of storing electrical

information.[18,74] This feature can be exploited in neuromorphic systems capable of mimicking human brain activity, as they can realize artificial neurons and synapses.[75]

As summarized in Table S2, Supporting Information, the devices exhibited a more significant variation in electrical performance compared to similar devices printed on pristine ACICC membrane, which can be attributed to the surface roughness. The performance of such devices can be significantly improved by performing better filtration of the remaining conductive carbon material. Despite this deviation in the device metrics, they exhibit electrical modulation of almost three orders of magnitude with $\mu_{Sat}$ of 4 $cm^2$ $V^{-1}$ $s^{-1}$ and $S_S$ of 0.5 V $dec^{-1}$.

## 3. Conclusions

In summary, the "dual-functionality" (physical support and dielectric) of the engineered nanopaper composite has revived a compelling concept of low-power paper electronics. The underlying science of the engineered nanopaper composite is based on merging the intrinsic mechanical, thermal and optical properties of micro/nanofibrous cellulose nanopaper, used as a reinforcing agent, with the electrochemical properties of a cellulose hydrogel electrolyte enriched with alkali metal ionic species, which confers high-capacitance and enhanced ionic conductivity to the composite. These materials yield a composite with tailored properties, including robustness, smooth surface, high-capacitance and reasonable transparency, which are not possible to achieve when used alone.

Such properties led us to explore its potential as a substrate and electrolyte-gate layer in low-voltage, fully screen-printed ZnO transistors and integrated logic gates. The planar architecture and "dual-functionality" of the nanopaper composite membrane simplifies the design of the devices, thus reducing their manufacturing cost, which is considerably lower when using printing/handwriting techniques.

The devices displayed good performance at low voltages below 2.5 V, showing mixed operating mode (field-effect and electrochemical doping mode), operating at switching speeds below 10 Hz. The elongated size of the ZnO particles ensures remarkable mechanical endurance upon bending/folding. Logic applications of the screen-printed NCGTs are also demonstrated, from simple inverters to "universal" logic gates, which operate at low input voltages of 3 V and present suitable gains for signal amplification.

Despite the short lifetime of the nanopaper-gated devices, they can be easily disintegrated in water to form a pulp that can be recycled and reused to produce new membranes to host iontronic devices, thus ensuring a resource-conscious mentality that fits into a circular economy model, where waste is treated as a resource. These exciting results may usher in a new era of low-power, foldable, printed iontronic devices with simplified designs.

## 4. Experimental Section

*Preparation of Cellulose Ionic Conductive Hydrogel Slurry*: Following the procedure reported in the authors' previous works,[32,33] a mixture of LiOH (Sigma-Aldrich, ≥98%) in urea (Carl Roth, ≥99.5%) and deionized water (Millipore), with a weight ratio of 4.6:15:80.4 (0.46 g of LiOH, 1.5 g of urea, and 8.04 g of water), was used as the solvent system in this study. The solvent mixture was precooled in a freezer at −25 °C, until it became a frozen solid. The frozen solution was then allowed to thaw at room temperature and 4 wt% of microcrystalline cellulose (MCC, 0.4 in 10 g of solution, Sigma-Aldrich, powder: 20 µm) was immediately added into the solvent system (9.6 in 10 g of solution) under vigorous stirring at −8 °C until its complete dissolution. To improve cellulose dissolution a freezing–thawing cycle was performed. A mixture of MCC and CMC (Sigma-Aldrich, $M_w \approx 250\,000$) with a weight ratio of 1:1 was prepared by adding 0.4 g of CMC to the previous cellulose solution (10 g). The mixture was stirred at room temperature conditions until CMC dissolution and then at −8 °C to ensure MCC dissolution. The transparent solution was kept overnight in a freezer at −25 °C. The last step consists of neutralization of the solution and simultaneous regeneration of cellulose with acetic acid (≈ 1 mL, Sigma-Aldrich, ≥99). This process was performed in an icy bath by slowly adding acetic acid drop-by-drop to the cellulose solution under stirring to avoid overheating. The resulting CICH slurry obtained was again stored in a freezer at −25 °C, overnight, until being used.

*Preparation of Iontronic Cellulose Nanopaper Composite*: Ionic conductive cellulose nanopaper composite was prepared by blending 5 wt% of CICH slurry (0.5 g) with 95 wt% of a cellulose pulp (0.95 g) provided from *Centre Technique du Papier*, consisting of an aqueous kraft pulp suspension containing 2 wt% of micro/nanofibrillated cellulose. The slow casting and evaporation of water was performed from 5 mL of the all-cellulose nanocomposite solution mixture in polystyrene Petri dishes (55 mm diameter) in a closed box with controlled environment (SICCO, T = 24 ± 2 °C, 33 ± 2 RH%) for 3 days and stored in air. Freestanding membranes were also prepared by solvent casting the micro/nanocellulose pulp without adding the CICH slurry (referred to as cellulose nanopaper), and by shear-casting the CICH slurry on a glass plate. Both membranes were obtained after drying in the same conditions as the ACICC membrane. A Mitutoyo digital micrometer was used to determine the thickness of the resulting cellulose nanopaper, ACICC and CICH membranes, which was estimated from the average of ten measurements ≈63.5 ± 1.59, ≈78.3 ± 0.78 and 336 ± 31.0 µm, respectively.

*Characterization of Cellulose-Based Membranes*: The optical transmittance measurements were performed with a Perkin Elmer Lambda 950 spectrophotometer in the wavelength range from 400 to 800 nm, with a scan of 1 nm and using air as the reference.

The membranes' morphology was characterized by SEM-EDS with a Carl Zeiss Auriga crossbeam (SEM-FIB) workstation instrument equipped with an Oxford EDS. The cellulosic membranes were attached on Al stubs using a double-sided carbon tape and coated with a thin iridium layer (<20 nm) using a Q300T D Quorum sputter coater.

The surface roughness of the cellulose-based membranes was analyzed by AFM and performed using an Asylum Research MFP-3D operated in alternate contact mode. The resolution of the image was 256 lines by 1024 columns and the scan size was 5 × 5 $\mu m^2$.

The structural analysis was done via X-ray diffraction (XRD, PANalytical, model X'Pert Pro) using a PANalytical X'Pert Pro, with Bragg–Brentano geometry and Cu K$\alpha$ line radiation ($\lambda$ = 1.5406 Å).

Fourier-transform infrared (FTIR) spectroscopy acquisitions were performed at room temperature, using an attenuated total reflectance sampling accessory (Smart iTR) equipped with a single-bounce diamond crystal on a Thermo Nicolet 6700 spectrometer. The spectra were acquired between 4000 and 650 $cm^{-1}$ with a 4 $cm^{-1}$.

Thermogravimetric analysis measurements were performed with a simultaneous thermal analyzer (TGA-DSC- STA449 F3 Jupiter). Approximately 3 mg of each sample was loaded into an Al pan and heated from 25 to 550 °C with a heating rate of 5 °C $min^{-1}$. All the measurements were carried out under air atmosphere.

Electrochemical characterization was carried out at room temperature (23 ± 2 °C, ≈ 40 RH%) using a Gamry Instruments Reference 600 potentiostat. The capacitance variation with frequency was investigated

by EIS with an AC excitation voltage of 10 mV rms in a frequency range of 0.1 to $10^6$ Hz. The electrochemical cell consists of a typical capacitor structure (carbon/membrane/carbon) with an active area of 1 $mm^2$. The materials were deposited in the same way as the EGTs, as described in the following section. CV measurements were performed in a potential range between −2.5 and 2.5 V and a collection of five successive cycles were acquired before analysis. To test the electrochemical stability of the oxide semiconductor, CV measurements were also performed including the semiconductor layer in the capacitors' structure: carbon/membrane/CMC:ZnO/carbon.

*Ink's Formulation*: The porous ZnO nanostructures were synthesized by the hydrothermal method assisted by microwave radiation, followed by a washing, drying, and calcination steps. The detailed description of the synthesis process is given by Ferreira et al.[55]

The prepared ZnO porous nanostructures were blended with a concentration of 30 wt% (3 g in a total of 10 g of ink) into a previously prepared solution of 3 wt% of CMC (0.3 g in water) dissolved in deionized water (9.7 g, Millipore). The mixture was slowly stirred (200 rpm) for 4 h to obtain a well dispersed and homogeneous white viscous solution. The ink was stored in a refrigerator at 3 °C, until being used.

*Fabrication of Planar Nanopaper Composite Gated Transistors*: Planar carbon electrodes were screen-printed on the smoothest side of the ACICC membrane using a conductive carbon paste (CRSN2644 C INK, Sun Chemical), and a screen mold made of polyester with the following conditions: mesh model, 120–34; mesh count, 305 mesh/inch; aperture, 45 µm; thread diameter, 34 µm; opening, 30.5%; fabric thickness, 52–57 µm. The carbon electrodes were dried at 70 °C for 15 min in air. Before printing the next layer, the membrane with the printed electrodes was stored for 1 h at ambient conditions to restore its moisture. The CMC/ZnO ink was screen-printed between the source and drain carbon electrodes ($W$ = 1 mm, $L$ = 200 µm, $W/L$ = 5) with a different polyester screen (mesh model: 77-55; mesh count: 190 mesh/inch; aperture: 81 µm; thread diameter: 55 µm; opening: 30%; thickness: 88–97 µm) and dried at room temperature in less than 10 s.

*Fabrication of Planar Nanopaper Composite Gated Logic Gates*: The ACICC membrane was glued with double-sided tape to a sheet of office paper (300%, Portucel Soporcel, Setúbal, Portugal). Graphitic line tracks were hand-drawn with a HB-2 pencil (Black'Peps, Maped) on the office paper to define the load resistances. The transistors were printed in the same way as described previously. After printing the planar carbon electrodes, thick carbon tracks were drawn with a brush to establish the electrical connections between the transistors and the load resistance, using the same ink to print the carbon electrodes. The screen-printed electrodes and hand-drawn tracks were dried simultaneously at 70 °C for 15 min in air. To conclude the circuits' fabrication, the ACICC membrane with the patterned carbon layers was stored for 1 h under ambient conditions, and then CMC/ZnO PNPs ink was screen-printed between the source and drain carbon electrodes, and dried at room temperature in less than 10 s.

*Biodegradability/Recycling Tests*: Nearly 0.2 g of ACICC membrane coated with printed devices was soaked in 9.8 g of water and then stirred for 24 h to obtain a homogeneous pulp of fibers. The pulp was used as raw material for the preparation of recycled membranes by performing solvent-casting in polystyrene Petri dishes (55 mm diameter) (Video S1, Supporting Information). The recycled membrane was prepared in the same conditions as the previous membranes, yielding a thickness of 50.1 ± 0.95 µm. AFM, SEM, EDS, EIS, and CV measurements were also performed on the recycled ACICC membrane. Screen-printed ZnO transistors were fabricated on the recycled membrane in the same conditions of the pristine membranes.

*Characterization of Nanopaper Composite Transistors and Integrated Circuits*: An optical microscope (Olympus BX51) was used to observe the surface topography of the devices. Images were processed using ImageJ software to estimate transistor's real dimensions from the average of 10 measurements. SEM images were also acquired.

The sheet resistance of the screen-printed carbon electrodes with a square shape of 1 $cm^2$ on ACICC membrane was determined by four-point probe technique (Jandel Engineering Ltd.) and estimated from the average of ten measurements.

The devices were electrically analyzed in the dark in air at room temperature (24 ± 2 °C, 38 ± 4 RH%) using a microprobe station (Cascade Microtech M150) connected to a semiconductor parameter analyzer (Agilent 4155C) controlled by the software Metrics ICS. In the case of the printed devices, they were tested 1 h after printing de semiconductor layer. For dynamic characterization, a microprobe station (Cascade Microtech MPS150) connected to a semiconductor parameter analyzer (Keysight B1500A) controlled by the software Keysight EasyEXPERT was used for biasing the circuit. A waveform generator was connected for input signal (Keysight 33500B Series).

## Supporting Information

Supporting Information is available from the Wiley Online Library or from the author.

## Acknowledgements

This work was financed by national funds from FCT – Fundação para a Ciência e a Tecnologia, I.P., in the scope of the projects LA/P/0037/2020, UIDP/50025/2020 and UIDB/50025/2020 of the Associate Laboratory Institute of Nanostructures, Nanomodelling and Nanofabrication – i3N, project CHIHC, reference PTDC/NAN-MAT/32558/2017, project CELLECTIVE, reference PTDC/CTM-CTM/4653/2021, the Ph.D. scholarships SFRH/BD/126409/2016 (I.C.) and SFRH/BD/122286/2016 (J.M.). S.H.F. acknowledges the support from the FCT – Fundação para a Ciência e a Tecnologia, I.P. through the AdvaMTech PhD program scholarship PD/BD/114086/2015. This work has received funding from the European Union's Horizon 2020 Research and Innovation Programme under the Grant Agreements Nos: 640598 (ERC-2014-STG NEW-FUN), 951774, (H2020-EIC-FETPROACT-2019 FOXES), 952169 (SYNERGY, H2020-WIDESPREAD-2020-5, CSA), and 101008701 (EMERGE, H2020-INFRAIA-2020-1). The authors would also like to thank their colleagues Daniela Gomes, Ana Pimentel, Sónia Pereira and Tomás Calmeiro from CENIMAT/i3N for the SEM, DSC-TGA, XRD and AFM measurements, respectively.

## Conflict of Interest

The authors declare no conflict of interest.

## Data Availability Statement

Research data are not shared.

## Keywords

foldable electronics, hydrogels, nanocellulose, paper electronics, printed electronics, sustainability, zinc oxide

Received: April 27, 2022
Revised: June 10, 2022
Published online: July 6, 2022

[1] M. Irimia-Vladu, *Chem. Soc. Rev.* **2014**, *43*, 588.
[2] S. Nandy, E. Fortunato, R. Martins, *Prog. Nat. Sci.: Mater. Int.* **2022**, *32*, 1.

[3] R. Martins, D. Gaspar, M. J. Mendes, L. Pereira, J. Martins, P. Bahubalindruni, P. Barquinha, E. Fortunato, *Appl. Mater. Today* **2018**, *12*, 402.
[4] D. Klemm, E. D. Cranston, D. Fischer, M. Gama, S. A. Kedzior, D. Kralisch, F. Kramer, T. Kondo, T. Lindström, S. Nietzsche, K. Petzold-Welcke, F. Rauchfuß, *Mater. Today* **2018**, *21*, 720.
[5] B. L. Tardy, B. D. Mattos, C. G. Otoni, M. Beaumont, J. Majoinen, T. Kämäräinen, O. J. Rojas, *Chem. Rev.* **2021**, *121*, 14088.
[6] H. Shaghaleh, X. Xu, S. Wang, *RSC Adv.* **2018**, *8*, 825.
[7] C. Lee, S. Kim, Y. Cho, *Adv. Sustainable Syst.* **2022**, *6*, 2000216.
[8] Y. Zhang, L. Zhang, K. Cui, S. Ge, X. Cheng, M. Yan, J. Yu, H. Liu, *Adv. Mater.* **2018**, *30*, 1801588.
[9] H. Zhu, W. Luo, P. N. Ciesielski, Z. Fang, J. Y. Zhu, G. Henriksson, M. E. Himmel, L. Hu, *Chem. Rev.* **2016**, *116*, 9305.
[10] A. T. Vicente, A. Araújo, M. J. Mendes, D. Nunes, M. J. Oliveira, O. Sanchez-Sobrado, M. P. Ferreira, H. Águas, E. Fortunato, R. Martins, *J. Mater. Chem. C* **2018**, *6*, 3143.
[11] D. Tobjörk, R. Österbacka, *Adv. Mater.* **2011**, *23*, 1935.
[12] Z. Shi, G. O. Phillips, G. Yang, *Nanoscale* **2013**, *5*, 3194.
[13] S. Nandy, S. Goswami, A. Marques, D. Gaspar, P. Grey, I. Cunha, D. Nunes, A. Pimentel, R. Igreja, P. Barquinha, L. Pereira, E. Fortunato, R. Martins, *Adv. Mater. Technol.* **2021**, *6*, 2000994.
[14] E. Fortunato, N. Correia, P. Barquinha, L. Pereira, G. Goncalves, R. Martins, *IEEE Electron Device Lett.* **2008**, *29*, 988.
[15] U. Zschieschang, H. Klauk, *J. Mater. Chem. C* **2019**, *7*, 5522.
[16] D. Gaspar, S. N. Fernandes, A. G. de Oliveira, J. G. Fernandes, P. Grey, R. V. Pontes, L. Pereira, R. Martins, M. H. Godinho, E. Fortunato, *Nanotechnology* **2014**, *25*, 094008.
[17] L. Pereira, D. Gaspar, D. Guerin, A. Delattre, E. Fortunato, R. Martins, *Nanotechnology* **2014**, *25*, 094007.
[18] R. Martins, P. Barquinha, L. Pereira, N. Correia, G. Gonçalves, I. Ferreira, E. Fortunato, *Appl. Phys. Lett.* **2008**, *93*, 203501.
[19] R. Martins, A. Nathan, R. Barros, L. Pereira, P. Barquinha, N. Correia, R. Costa, A. Ahnood, I. Ferreira, E. Fortunato, *Adv. Mater.* **2011**, *23*, 4491.
[20] R. F. P. Martins, A. Ahnood, N. Correia, L. M. N. P. Pereira, R. Barros, P. M. C. B. Barquinha, R. Costa, I. M. M. Ferreira, A. Nathan, E. E. M. C. Fortunato, *Adv. Funct. Mater.* **2013**, *23*, 2153.
[21] P. Grey, D. Gaspar, I. Cunha, R. Barras, J. T. Carvalho, J. R. Ribas, E. Fortunato, R. Martins, L. Pereira, *Adv. Mater. Technol.* **2017**, *2*, 1700009.
[22] T. H. Nguyen, A. Fraiwan, S. Choi, *Biosens. Bioelectron.* **2014**, *54*, 640.
[23] D. Ha, Z. Fang, N. B. Zhitenev, *Adv. Electron. Mater.* **2018**, *4*, 1700593.
[24] I. Ferreira, B. Brás, J. I. Martins, N. Correia, P. Barquinha, E. Fortunato, R. Martins, *Electrochim. Acta* **2011**, *56*, 1099.
[25] Y. Zhou, C. Fuentes-Hernandez, T. M. Khan, J.-C. Liu, J. Hsu, J. W. Shim, A. Dindar, J. P. Youngblood, R. J. Moon, B. Kippelen, *Sci. Rep.* **2013**, *3*, 1536.
[26] A. S. Adila, A. Husam, G. Husi, in 2018 2nd Int. Symp. Small-Scale Intell. Manuf. Syst. (SIMS), IEEE, Cavan, Ireland **2018**, pp. 1–5.
[27] V. Pecunia, L. G. Occhipinti, R. L. Z. Hoye, *Adv. Energy Mater.* **2021**, *11*, 2100698.
[28] S. H. Kim, K. Hong, W. Xie, K. H. Lee, S. Zhang, T. P. Lodge, C. D. Frisbie, *Adv. Mater.* **2013**, *25*, 1822.
[29] S. Z. Bisri, S. Shimizu, M. Nakano, Y. Iwasa, *Adv. Mater.* **2017**, *29*, 1607054.
[30] H. Du, X. Lin, Z. Xu, D. Chu, *J. Mater. Sci.* **2015**, *50*, 5641.
[31] S. Thiemann, S. J. Sachnov, F. Pettersson, R. Bollström, R. Österbacka, P. Wasserscheid, J. Zaumseil, *Adv. Funct. Mater.* **2014**, *24*, 625.
[32] I. Cunha, R. Barras, P. Grey, D. Gaspar, E. Fortunato, R. Martins, L. Pereira, *Adv. Funct. Mater.* **2017**, *27*, 1606755.
[33] I. Cunha, J. Martins, D. Gaspar, P. G. Bahubalindruni, E. Fortunato, R. Martins, L. Pereira, *Adv. Electron. Mater.* **2021**, *7*, 2001166.
[34] S. Khan, L. Lorenzelli, R. S. Dahiya, *IEEE Sens. J.* **2015**, *15*, 3164.
[35] I. Cunha, J. Martins, P. G. Bahubalindruni, J. T. Carvalho, J. Rodrigues, S. Rubin, E. Fortunato, R. Martins, L. Pereira, *Adv. Mater. Technol.* **2021**, *6*, 2100633.
[36] S. H. Ferreira, I. Cunha, J. V. Pinto, J. P. Neto, L. Pereira, E. Fortunato, R. Martins, *Chemosensors* **2021**, *9*, 192.
[37] P. I. C. Claro, A. C. Marques, I. Cunha, R. F. P. Martins, L. M. N. Pereira, J. M. Marconcini, L. H. C. Mattoso, E. Fortunato, *ACS Appl. Nano Mater.* **2021**, *4*, 8262.
[38] F. Foroughi, E. Rezvani Ghomi, F. Morshedi Dehaghi, R. Borayek, S. Ramakrishna, *Materials* **2021**, *14*, 714.
[39] H. Zhu, Z. Fang, C. Preston, Y. Li, L. Hu, *Energy Environ. Sci.* **2014**, *7*, 269.
[40] Z. Fang, H. Zhang, S. Qiu, Y. Kuang, J. Zhou, Y. Lan, C. Sun, G. Li, S. Gong, Z. Ma, *Adv. Mater. Technol.* **2021**, *6*, 2000928.
[41] J. Cai, L. Zhang, *Macromol. Biosci.* **2005**, *5*, 539.
[42] S. Gan, S. Zakaria, C. H. Chia, R. S. Chen, A. V. Ellis, H. Kaco, *PLoS One* **2017**, *12*, e0173743.
[43] E. J. Foster, R. J. Moon, U. P. Agarwal, M. J. Bortner, J. Bras, S. Camarero-Espinosa, K. J. Chan, M. J. D. Clift, E. D. Cranston, S. J. Eichhorn, D. M. Fox, W. Y. Hamad, L. Heux, B. Jean, M. Korey, W. Nieh, K. J. Ong, M. S. Reid, S. Renneckar, R. Roberts, J. A. Shatkin, J. Simonsen, K. Stinson-Bagby, N. Wanasekara, J. Youngblood, *Chem. Soc. Rev.* **2018**, *47*, 2609.
[44] L. Segal, J. J. Creely, A. E. Martin, C. M. Conrad, *Text. Res. J.* **1959**, *29*, 786.
[45] S. Park, J. O. Baker, M. E. Himmel, P. A. Parilla, D. K. Johnson, *Biotechnol. Biofuels* **2010**, *3*, 10.
[46] J. Łojewska, P. Miśkowiec, T. Łojewski, L. M. Proniewicz, *Polym. Degrad. Stab.* **2005**, *88*, 512.
[47] A. M. Olsson, L. Salmén, *Carbohydr. Res.* **2004**, *339*, 813.
[48] S. Y. Oh, I. Y. Dong, Y. Shin, C. K. Hwan, Y. K. Hak, S. C. Yong, H. P. Won, H. Y. Ji, *Carbohydr. Res.* **2005**, *340*, 2376.
[49] J. X. Sun, X. F. Sun, H. Zhao, R. C. Sun, *Polym. Degrad. Stab.* **2004**, *84*, 331.
[50] F. Shao, P. Feng, C. Wan, X. Wan, Y. Yang, Y. Shi, Q. Wan, *Adv. Electron. Mater.* **2017**, *3*, 1600509.
[51] P. F. Moonen, I. Yakimets, J. Huskens, *Adv. Mater.* **2012**, *24*, 5526.
[52] S. M. F. Cruz, L. A. Rocha, J. C. Viana, in *Flexible Electron.*, InTech, **2018**, p. 13.
[53] S. Thiemann, M. Gruber, I. Lokteva, J. Hirschmann, M. Halik, J. Zaumseil, *ACS Appl. Mater. Interfaces* **2013**, *5*, 1656.
[54] H. Yang, S.-Q. Ni, X. Jiang, W. Jiang, J. Zhan, *CrystEngComm* **2012**, *14*, 6023.
[55] S. H. Ferreira, M. Morais, D. Nunes, M. J. Oliveira, A. Rovisco, A. Pimentel, H. Águas, E. Fortunato, R. Martins, *Materials* **2021**, *14*, 2385.
[56] S. H. Ferreira, A. Rovisco, A. dos Santos, H. Águas, R. Igreja, P. Barquinha, E. Fortunato, R. Martins, in *Nanopores*, IntechOpen, **2021**, p. 13.
[57] C.-F. Liu, Y.-J. Lu, C.-C. Hu, *ACS Omega* **2018**, *3*, 3429.
[58] Y. J. Tak, S. T. Keene, B. H. Kang, W.-G. Kim, S. J. Kim, A. Salleo, H. J. Kim, *ACS Appl. Mater. Interfaces* **2020**, *12*, 2615.
[59] D. Ho, H. Jeong, S. Choi, C. Kim, *J. Mater. Chem. C* **2020**, *8*, 14983.
[60] J. Carvalho, V. Dubceac, P. Grey, I. Cunha, E. Fortunato, R. Martins, A. Clausner, E. Zschech, L. Pereira, *Nanomaterials* **2019**, *9*, 169.
[61] D. Gaspar, J. Martins, P. Bahubalindruni, L. Pereira, E. Fortunato, R. Martins, *Adv. Electron. Mater.* **2018**, *4*, 1800423.
[62] W. J. Hyun, E. B. Secor, G. A. Rojas, M. C. Hersam, L. F. Francis, C. D. Frisbie, *Adv. Mater.* **2015**, *27*, 7058.
[63] N. Kurra, G. U. Kulkarni, *Lab Chip* **2013**, *13*, 2866.
[64] K. Hong, S. H. Kim, K. H. Lee, C. D. Frisbie, *Adv. Mater.* **2013**, *25*, 3413.

[65] Y. Cao, K. E. Uhrich, *J. Bioact. Compat. Polym.* **2019**, *34*, 3.
[66] N. X. Williams, G. Bullard, N. Brooke, M. J. Therien, A. D. Franklin, *Nat. Electron.* **2021**, *4*, 261.
[67] F. B. Kadumudi, J. Trifol, M. Jahanshahi, T.-G. Zsurzsan, M. Mehrali, E. Zeqiraj, H. Shaki, M. Alehosseini, C. Gundlach, Q. Li, M. Dong, M. Akbari, A. Knott, K. Almdal, A. Dolatshahi-Pirouz, *ACS Appl. Mater. Interfaces* **2020**, *12*, 48027.
[68] S. W. Hwang, D. H. Kim, H. Tao, T. Il Kim, S. Kim, K. J. Yu, B. Panilaitis, J. W. Jeong, J. K. Song, F. G. Omenetto, J. A. Rogers, *Adv. Funct. Mater.* **2013**, *23*, 4087.
[69] C. Dagdeviren, S. W. Hwang, Y. Su, S. Kim, H. Cheng, O. Gur, R. Haney, F. G. Omenetto, Y. Huang, J. A. Rogers, *Small* **2013**, *9*, 3398.
[70] J. Guo, J. Liu, B. Yang, G. Zhan, X. Kang, H. Tian, L. Tang, X. Chen, C. Yang, *IEEE Electron Device Lett.* **2015**, *36*, 576.
[71] H. Cheng, V. Vepachedu, *Theor. Appl. Mech. Lett.* **2016**, *6*, 21.
[72] P. Grey, S. N. Fernandes, D. Gaspar, J. Deuermeier, R. Martins, E. Fortunato, M. H. Godinho, L. Pereira, *ACS Appl. Electron. Mater.* **2020**, *2*, 426.
[73] N. Pullanjiot, S. Swaminathan, *Sol. Energy* **2019**, *186*, 37.
[74] R. Martins, L. Pereira, P. Barquinha, N. Correia, G. Gonçalves, I. Ferreira, C. Dias, N. Correia, M. Dionísio, M. Silva, E. Fortunato, *J. Inf. Disp.* **2009**, *10*, 149.
[75] N. K. Upadhyay, H. Jiang, Z. Wang, S. Asapu, Q. Xia, J. J. Yang, *Adv. Mater. Technol.* **2019**, *4*, 1800589.